Red-Light Photocatalytic Activation Of Pt(IV) Anticancer Prodrugs Using Methylene Blue

Ana C. Carrasco,[1#] Greta Bajetto[2,3#], Stefano Scoditti,[4*] German E. Pieslinger,[1,5] Francesco Gambino,[1] Marco De Andrea[2,3], Emilia Sicilia,[4] Virginia Martínez-Martínez,[6*] Valentina Dell'Oste,[2*] Luca Salassa[1,7,8*]

[1] *Donostia International Physics Center, Paseo Manuel de Lardizabal 4, Donostia, 20018, Spain*

[2] *Department of Public Health and Pediatric Sciences, University of Turin, Turin, Italy*

[3] *CAAD Center for Translational Research on Autoimmune and Allergic Disease, University of Piemonte Orientale, Novara Medical School, Novara, Italy*

[4] *Department of Chemistry and Chemical Technologies, University of Calabria, Arcavacata di Rende (CS), 87036, Italy*

[5] *CONICET – Universidad de Buenos Aires, Instituto de Química y Fisicoquímica Biológicas (IQUIFIB), Buenos Aires,* 1113*, Argentina*

[6] *Departamento de Química Física, Universidad del País Vasco, UPV/EHU, Apartado 644, Bilbao, 48080, Spain*

[7] *Polimero eta Material Aurreratuak: Fisika, Kimika eta Teknologia, Kimika Fakultatea, Euskal Herriko Unibertsitatea UPV/EHU, Paseo Manuel de Lardizabal 3, Donostia, 20018, Spain*

[8] *Ikerbasque, Basque Foundation for Science, Bilbao, 48011, Spain*

 # contributed equally

Abstract. Catalysis-based approaches offer versatile strategies for activating anticancer prodrugs, potentially allowing precise control over drug release and localization within tumor tissues, while reducing systemic toxicity. In this study, we explore the role of the phenothiazine dye methylene blue (**MB**$^+$) as a photocatalyst in conjunction with biologically relevant electron donors to facilitate the red-light conversion of two Pt(IV) complexes, denoted as *cis,cis,trans*-$[PtCl_2(NH_3)_2(O_2CCH_2CH_2COOH)_2]$ (**1**) and *trans*-$[Pt(O_2CCH_2CH_2COOH)_2$*1R,2R*-(DACH)(ox)] (**2**), into cisplatin and oxaliplatin, respectively. Combining spectroscopic techniques (NMR, UV-Vis, flash photolysis) with computational methods, we reveal that the doubly reduced **MB**$^+$ (leucomethylene blue, **LMB**) triggers the reductive elimination of axial ligands in the two Pt(IV) precursors, generating the corresponding Pt(II) anticancer drugs.
In vitro experiments conducted on the human cervical cancer cell line CaSki, which harbors multiple copies of the integrated HPV-16 genome, and on non-tumoral cells (HaCat) demonstrate that co-administration with Pt(IV) prodrugs improves **MB**$^+$'s antiproliferative efficacy in cancer cells, particularly under red light exposure. This enhancement could be attributed to the catalytic production of Pt(II) species within the cellular environment.

Introduction

Chemists have significantly improved their ability to develop non-natural metal-based catalytic reactions for use in biological settings over the past decade.[1–3] Such catalysis schemes are geared towards fundamental purposes, developing innovative biology tools, and exploring novel imaging and therapy approaches.[4–7]

In the therapy domain, alongside PDT (photodynamic therapy) using photosensitizers as catalysts to produce singlet oxygen in biological systems,[8] metallodrugs have shown potential to exert anticancer effects by catalytically altering key biological components like DNA, proteins,[5,9–11] and essential metabolites. [12–14]
In these applications, catalysis plays a critical role in accelerating reaction rates, amplifying chemical signals, and ensuring selectivity. This is essential for triggering or quickly detecting chemical responses, limiting side reactions, enhancing biological effects within a confined timeframe, and gaining insights into biological processes.

In our research, we have discovered that flavins and flavoproteins, both in their natural and synthetic forms, possess the ability to photocatalyze the conversion of Pt(IV) anticancer prodrugs into clinically approved Pt(II) drugs in the presence of electron donors.[15–20] Unlike conventional catalysis, where metal complexes typically act as catalysts, in these reactions, they serve as substrates.[21] Flavin reactivity towards Pt(IV) complexes demonstrates remarkable selectivity and efficiency, particularly in terms of turnover number and frequency. Such factors are crucial for catalysis-based therapies to ensure timely substrate transformation and mitigate clearance or off-target effects. Besides, employing light activation and excited-state chemistry offers an unparalleled means to enhance reaction rates.[19]

A limitation of flavin-catalyzed activation of Pt(IV) prodrugs is the necessity for blue light sources for photoirradiation.[20] The absorption profile of flavins restricts the wavelength range, which is suboptimal for tissue penetration. Therefore, it is desirable to shift the excitation wavelength of the catalyst towards the red and near-infrared range, within the therapeutic window of the visible spectrum, which offers greater tissue penetration and reduced damage to cellular components.[8]
For this purpose, we explored alternative photocatalysts with (photo)redox capabilities akin to flavins but functional in longer wavelength conditions. One promising candidate was methylene blue (**MB**$^+$), a phenothiazine dye absorbing light in the 600-700 nm range, capable of both single-electron and double-electron reductions with electron donors. Moreover, **MB**$^+$ has a rich medical history of treating chemical poisoning,[22] infections,[23] and Alzheimer's disease.[24] It is currently used clinically for methemoglobinemia[25] and has gained attention for cancer imaging and therapy, especially in PDT schemes.[26,27] This is evidenced by the multitude of clinical trials carried out worldwide exploring **MB**$^+$ efficacy in this domain.[28]
In this study, we demonstrate how **MB**$^+$ efficiently catalyzes the conversion of two Pt(IV) complexes into their active Pt(II) forms, cisplatin and oxaliplatin, under red light and in the presence of bioreductants (Figure 1). Combining experimental and theoretical methods, we elucidate the mechanism where the doubly reduced form of **MB**$^+$, known as leucomethylene blue (**LMB**), acts as the catalyst for Pt(IV) activation. Our *in vitro* investigations on both healthy and cancer cells show that this photocatalytic approach enhances the PDT efficacy of **MB**$^+$ by likely generating anticancer Pt(II) drugs within the cells.

Results and discussion

Catalysis experiments

We explored the capacity of **MB**$^+$ to catalytically convert Pt(IV) prodrugs into their active Pt(II) analogs in the presence of bioreductants such as NADH, glutathione (GSH), and sodium ascorbate (NaAsc). Complexes *cis,cis,trans*-$[PtCl_2(NH_3)_2(O_2CCH_2CH_2COOH)_2]$ (**1**) and *trans*-$[Pt(O_2CCH_2CH_2COOH)_2$*1R,2R*-

(DACH)(ox)] (**2**, DACH = *trans*-1,2-diaminocyclohexane and ox = oxalate) were selected for this task as biologically inactive precursors of cisplatin and oxaliplatin respectively (Figure 1, Figure S1 and S2).[29] Initially, we screened the catalytic reactions in PBS (10 mM, pH 7.4) by ^{1}H NMR using a 2 mM electron donor, 500 µM Pt substrate, and 25 µM **MB**$^{+}$ (5% catalyst loading). Progression of the reaction was monitored following the changes relative to the ^{1}H NMR signals of the Pt-coordinated and free succinate axial ligands. We compared samples in the dark and irradiated at 650 nm (30 min, 0.1 mW·cm^{-2}) to have a first estimate of the conversion efficiency (Figure 2). Additional controls included **1** and **2** alone and in combination with either **MB**$^{+}$ or the electron donors under light irradiation and in the dark (Figure S3–7).

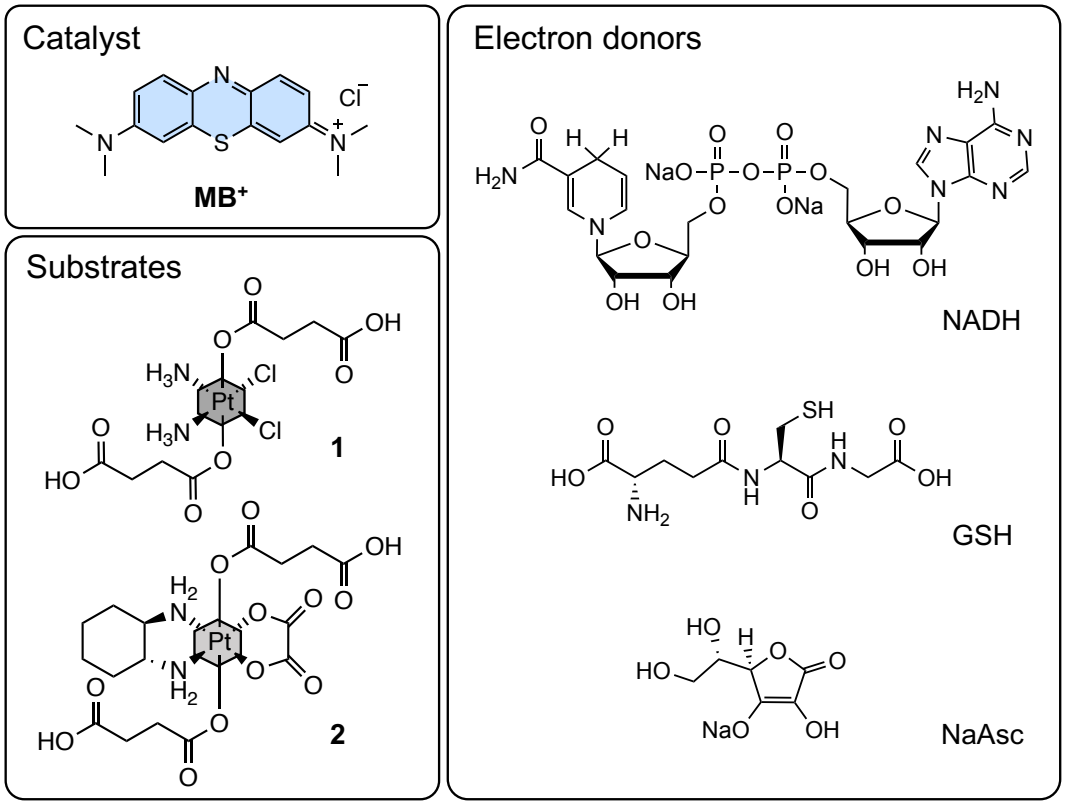

Figure 1. Schematic structures of the catalyst, Pt(IV) substrates and electron donors employed in this work.

Under the described conditions, we found that the photocatalytic efficiency of **MB**$^{+}$ towards the activation of Pt(IV) complexes followed the order NADH > NaAsc > GSH (Figure 2, Figure S8a and S8b). NADH was capable of generating the Pt(II) drugs in the dark as well, although at a slow rate. Conversely, exposure to red light facilitated the rapid conversion of the Pt substrates, achieving approximately 85% conversion within 30 minutes of irradiation. GSH was the least active donor inducing no formation of cisplatin or oxaliplatin in the dark, and ~16% conversion for **1** upon 1 h of red-light exposure. GSH did not activate **2** in the experimental timeframe, likely because of the higher thermodynamic stability of this metal complex. These findings agree with work from the 80's by Alexander and Kelner who reported that **MB**$^{+}$ oxidized GSH 12 times slower compared to NADPH.[30] In the case of NaAsc, prodrug activation in the dark is slower than for NADH, with **1** and **2** reaching full conversion within 24 h. Instead, photoirradiation prompted ~46% conversion of the Pt(IV) complexes after 30 min and 69% after 1 h in the case of **1**. Only 13% conversion was instead observed for **2** upon 1 h of red-light exposure.

Additionally, we conducted catalysis experiments with varying concentrations of **MB**$^+$ (1–100 μM, Figure S8c) in the presence of NADH (2 mM) and **1** (500 μM). The results revealed turnover numbers and frequencies, reaching 40 and 0.42 min^{-1}, respectively, at catalyst loadings of 10% and 25%. Notably, the former value was achieved after 60 minutes of red-light irradiation, while the latter occurred after 20 minutes, corresponding to approximately 40% substrate conversion.

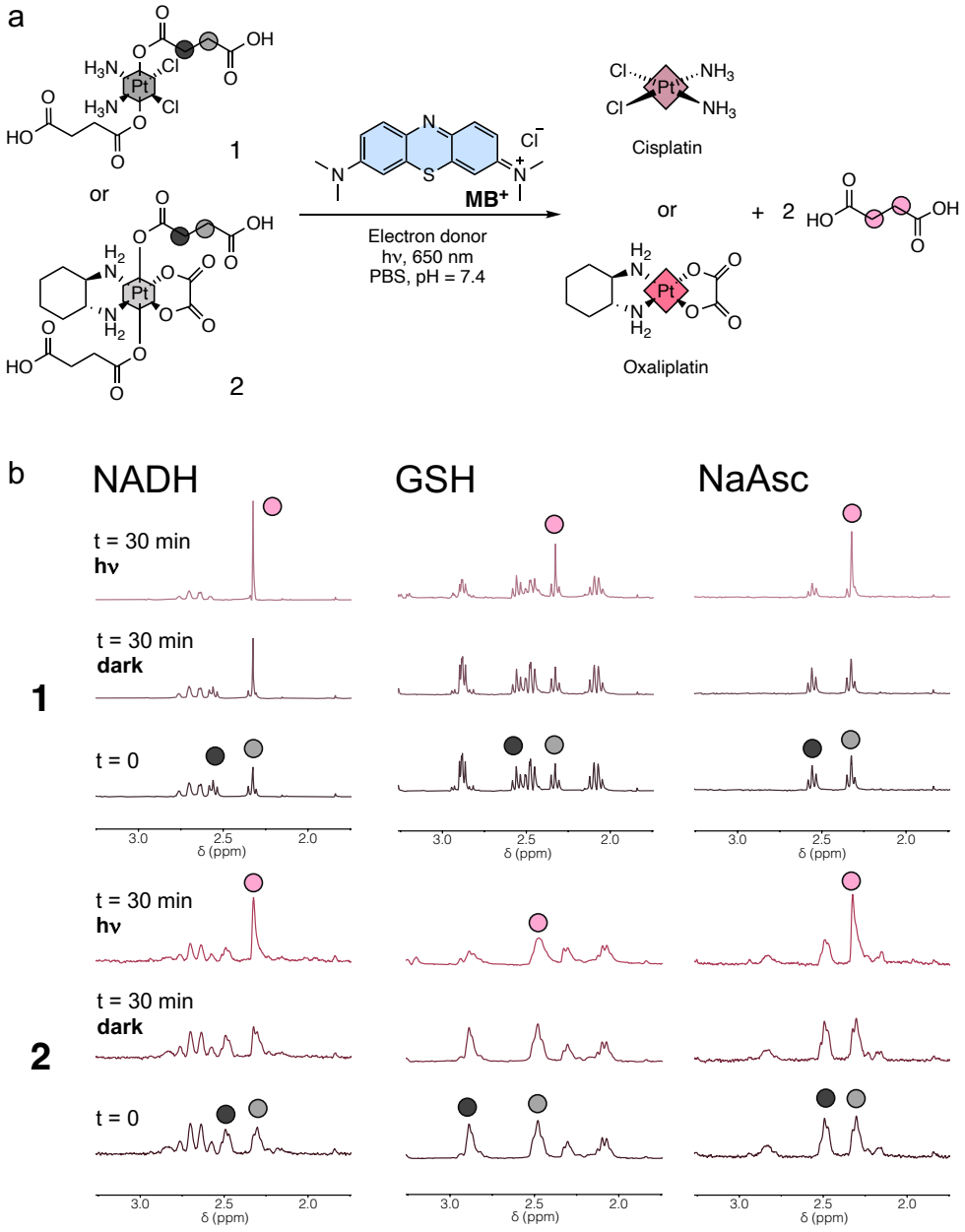

Figure 2. (a) Catalytic reduction of **1** and **2** to cisplatin and oxaliplatin, respectively, promoted by **MB**$^+$ in the presence of electron donors (NADH, GSH, and NaAsc); (b) ^{1}H NMR spectra (selected region) showing the reaction progression for **1** and **2** in the dark and upon light irradiation. Reaction conditions: 500 μM **1** or **2**, 2 mM electron donor, 25 μM **MB**$^+$ in PBS/D_2O (9:1, 10 mM, pH = 7.4); λ_{exc} = 650 nm (0.1 mW·cm^{-2}). ^{1}H-NMR signal labelling: ● Pt–OCO$\underline{CH_2}$CH$_2$CO$_2$H; ● Pt–OCOCH$_2\underline{CH_2}$CO$_2$H; ● free HO$_2$CCH$_2$CH$_2$CO$_2$H.

^{195}Pt NMR of photoirradiated samples confirmed that catalysis in the presence of NADH and NaAsc delivered the expected Pt(II) anticancer drugs as previously observed for flavin catalysts,[29,31] but not necessarily for other photoactivation modalities (Figure S9).[32] We also performed experiments with glucose as an electron donor since its capacity to

reduce **MB**$^+$ has been extensively demonstrated, for example in the so-called "blue bottle" experiment.[33] Nevertheless, we found no conversion of the Pt substrates at pH 7.4, but only at highly basic pH values (Figure S10).

Reaction in cell culture media

We evaluated the effectiveness of **MB**$^+$ as a catalyst in a challenging environment like cell culture medium (Figure S11-S14). We utilized phenol-red-free RPMI and DMEM media supplemented with 10% FBS (fetal bovine serum) and employed the same incubation and photoirradiation intervals used in the *in vitro* experiments (vide infra). Complexes **1** and **2** (500 μM) remained stable when dissolved in RPMI and DMEM media for 3 h in the absence of **MB**$^+$. In such instances, 30 minutes of photoirradiation did not induce any significant changes in the complexes. Similarly, no conversion of **1** and **2** was observed in the dark for reactions containing **MB**$^+$ (25 μM). However, the release of succinate ligands and activation of the complexes were evident in **MB**$^+$-containing samples that were photoirradiated for 30 min with red light. Complex **1** was converted more efficiently than complex **2** in both types of medium.

Catalytic mechanism

We employed time-resolved fluorescence and flash photolysis to assess the role of **MB**$^+$ singlet and triplet excited states in the photocatalytic activation of Pt(IV) substrates. Time Dependent-Density Functional Theory (TD-DFT) calculations aided in assigning the **MB**$^+$ species involved in the photochemical process (Figure S15).

Fluorescence spectra of **MB**$^+$ (4 μM, 0.1 OD) in PBS were collected by exciting at 615 nm without purging O_2. Confirming previous reports,[34] the emission peak centered at 687 nm displayed a lifetime of 0.368 ns. None of the tested electron donors (80-fold excess) had a significant quenching effect on the ^{1}**MB**$^+$ lifetime, even when a Pt substrate was simultaneously added. This indicated that the lowest excited singlet state (S_1) was not a major actor in the catalytic process (Figure S16).

Next, we evaluated the effect of the electron donors on the ^{3}**MB**$^{+*}$ state by absorption transient spectroscopy monitoring the decay of the characteristic triplet absorption band at 824 nm (λ_{exc} = 615 nm, 12 μM **MB**$^+$ in PBS, 0.35 OD, Figure 3a). In agreement with reported data,[35,36] air-saturated solutions of **MB**$^+$ alone showed a triplet lifetime of 1.3 μs ($\tau_{T\text{-}Air}$), whereas the value increased to 8 μs under an N_2 atmosphere ($\tau_{T\text{-}N2}$), Figure 3b.

When an excess of NADH was employed (Figure 3c), $\tau_{T\text{-}Air}$ dropped to 0.23 μs consistently with the two-electron quenching of ^{3}**MB**$^{+*}$ and formation of leucomethylene blue (**LMB**). Decay traces in N_2 atmosphere could not be carried out since the sample instantaneously became colorless upon exposure to the excitation laser beam.

When GSH was employed as an electron donor (Figure 3d), $\tau_{T\text{-}Air}$ and $\tau_{T\text{-}N2}$ were reduced compared to **MB**$^+$ alone to approximately 1.1 μs and 3.2 μs respectively. The result is in agreement with the generation of **LMB** via quenching of ^{3}**MB**$^{+*}$. In line with the modest catalytic performance of **MB**$^+$ in the presence of GSH, the process exhibited poor efficiency. This was evident in the solution's persistent blue color, which failed to turn colorless even after prolonged light irradiation, and in the minimal change observed in triplet lifetimes (Figure 3d *vs* 3b).

In the case of NaAsc (Figure 3e and Figure S17), ^{3}**MB**$^{+*}$ absorption at 824 nm displayed a bi-exponential decay for $\tau_{T\text{-}air}$, with a short (20%) and a long (80%) component of 150 ns and 95 μs, respectively, with the latter slightly increasing to 130 μs in a deaerated solution ($\tau_{T\text{-}N2}$). Previous work established that ascorbate is capable of reducing light-excited **MB**$^+$ to **LMB** via a two-step radical mechanism.[37] Therefore, the short τ could

be assigned to the quenching of ^{3}**MB^{+*}** by ascorbate whereas the long component to an **MB$^+$** radical species (**MB•**). This assignment aligns with Time-dependent Density Functional Theory (TD-DFT) which predicts that **MB•** has absorption features in the same wavelength range (Figure S15). Ascorbate and/or its radical form could engage in a second single electron transfer with **MB•**, ultimately generating **LMB**. Control experiments with the radical scavenger TEMPO showed that **MB$^+$** activity towards **1** remains nearly unaffected, suggesting that the **MB•** species is only marginally involved in the catalytic mechanism (Figure S18).

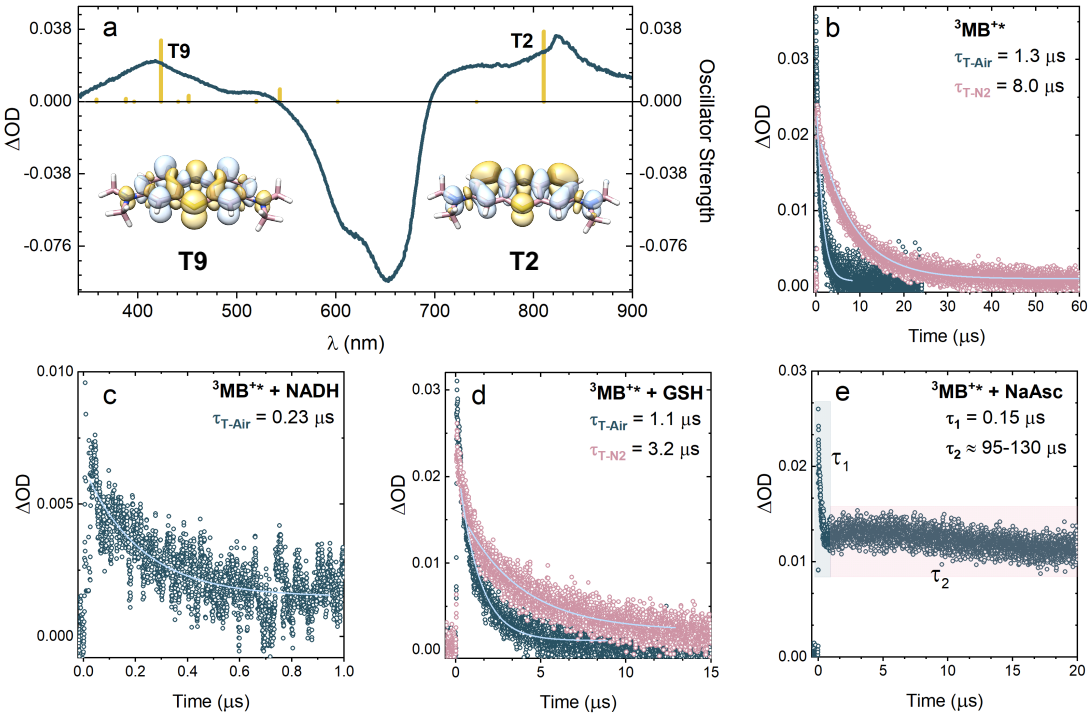

Figure 3. (a) Transient absorption spectrum of ^{3}**MB^{+*}** (λ_{exc} = 615 nm, 12 μM **MB$^+$**) and TD-DFT triplet-triplet transitions calculated at the B3LYP/def2-TZVPPD level (yellow vertical bars). The nature of the electronic transition T2 and T9 are described by means of their corresponding electron density difference maps (EDDMs), where light blue and yellow areas indicate a loss and a gain in electron density, respectively; (b-e) decays of the triplet–triplet absorption at 824 nm for ^{3}**MB^{+*}** alone and in the presence of different electron donors (80-fold excess,10 mM PBS, pH = 7.4).

The involvement of **LMB** in the Pt(IV) activation process was further supported by UV-Vis spectroscopy under anaerobic conditions (N_2 atmosphere). Upon co-incubation of **MB$^+$** and NADH (24:80 μM) under light irradiation, the solution rapidly decolorized, consistent with the disappearance of the absorption band at 660 nm and the formation of **LMB** (Figure 4a).[38] Similar results were observed for NaAsc (Figure S19), while GSH failed to bleach the **MB$^+$** solution. When **1** (6-12 equivalents) was added to the colorless solution under anaerobic conditions, it gradually reverted to blue, indicating the oxidation of **LMB** to **MB$^+$** and the conversion of the Pt prodrug to cisplatin. This conclusion was further supported by ^{1}H NMR spectroscopy in PBS/D_2O. Figure 4b shows that the resonances of **MB$^+$** (1 mM) partially disappeared upon **LMB** formation and reappeared upon the addition of an excess of the Pt substrate (8 mM) relative to NADH (4 mM). The signal of the free succinate obtained from the activation of **1** confirmed the formation of cisplatin. Full conversion of **1** was observed when its concentration was substoichiometric compared to the electron donor (Figure S20). Consistent with previous observations for reduced flavins,[20] **LMB** resonances were not

detectable in ^{1}H NMR, likely due to the rapid proton exchange of the NH group with solvent water molecules.

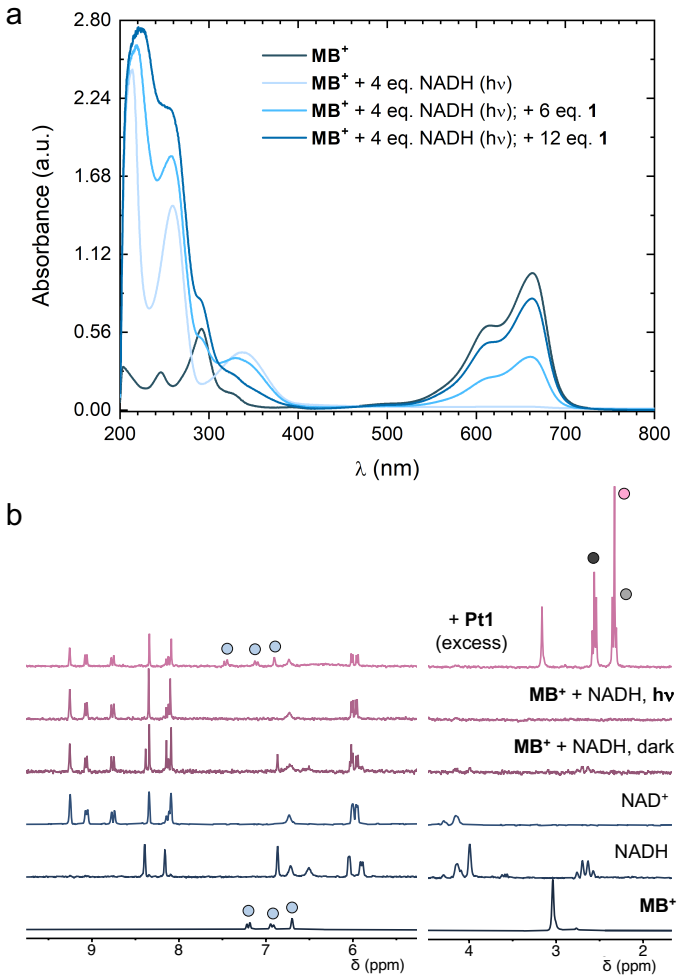

Figure 4. (a) Absorption and (b) ^{1}H NMR spectra of photoirradiated **MB**$^{+}$ in the presence of NADH and **1** (PBS 10 mM, pH= 7.4). Samples were treated with a light-emitting diode (LED) (λ_{irrad}= 650 nm, 0.1 mW cm^{-2}, 10 min). ^{1}H-NMR signal labelling: ● Pt–OCO*CH*$_2$CH$_2$CO$_2$H; ● Pt–OCOCH$_2$*CH*$_2$CO$_2$H; ● free HO$_2$CCH$_2$CH$_2$CO$_2$H; ● **MB**$^{+}$.

According to the sum of these data, a plausible catalytic mechanism entails i) the generation of ^{3}**MB**$^{+\ast}$ by light excitation, ii) the reductive quenching of ^{3}**MB**$^{+\ast}$ by electron donors and the subsequent formation of **LMB** (active catalyst), iii) the reductive elimination reaction of the Pt(IV) substrate promoted by **LMB** and the restoration of **MB**$^{+}$. We employed density functional theory (DFT) to validate this hypothesis. Our study modeled the behavior of **MB**$^{+}$ in the presence of NADH, exploring its two-electron reduction to **LMB** through both singlet ground-state (dark) and triplet-excited state (light-activated) pathways (Figure S21a). Additionally, we investigated the activation reaction of substrate **2** by **LMB** (Figure 5 and Figure S22). We excluded NaAsc and GSH due to their complex modeling requirements, which are beyond the scope of this manuscript. Computational work was performed adopting the methodology recently described by us to investigate the flavin-catalyzed activation of Pt(IV) anticancer prodrugs.[39] In all the calculations, the protonation states of **MB**$^{+}$ and **LMB** (PBS, pH = 7.4) were considered according to literature values.[40]

Singlet and triplet energy profiles determined for the reduction of **MB**$^{+}$ by NADH display a strong similarity to what was recently found for riboflavin.[39] As shown in Figure S21b, π-π interactions between the NADH nicotinic ring and **MB**$^{+}$ favor the formation of a

$^{1/3}$[NADH:**MB**$^{+}$] complex from which reduction to afford **LMB** can take place. Molecular Orbital (MO) analysis of the adduct in the singlet ground state suggests that this is indeed the case since the HOMO of ^{1}[NADH:**MB**$^{+}$] is located on the nicotinic ring of NADH while LUMO is centered on **MB**$^{+}$ (Figure S21c). Such a pathway involves a hydride transfer through a transition state (^{1}TS) whose energy is 16.3 kcal·mol^{-1} higher than the entrance channel ^{1}[NADH:**MB**$^{+}$]. The reaction is exergonic, resulting in a product that is 8.4 kcal·mol^{-1} more stable than the initial adduct. Hydride transfer and the formation of **LMB** are confirmed by the loss of planarity in the structure of the phenothiazine moiety (Figure S21c).[41] In the triplet state, the spin density surface of ^{3}[NADH:**MB**$^{+}$] is spread on both molecules indicating that an instantaneous 1-electron transfer takes place upon light irradiation (Figure S21d). In a subsequent step, the H-transfer through the nicotinic ring to **MB**$^{+}$ exhibits a remarkably low barrier (3.6 kcal·mol^{-1}, ^{3}TS). The resulting product is significantly stabilized (17.9 kcal·mol^{-1}) compared to the triplet entrance channel. These findings confirm that the reduction of **MB**$^{+}$ can occur even without light irradiation. However, the application of light triggers an alternative mechanism that accelerates the formation of the active catalyst **LMB**.

Next, we modeled the reductive elimination reaction of **2** by **LMB** which affords the Pt(II) drug oxaliplatin. Free energy profiles were determined for both **LMB** and its deprotonated form at the phenothiazine N–H site (**LMB**$^{-}$). The pKa of **LMB** in aqueous solution is 5.9,[40] therefore **LMB**$^{-}$ is the dominating species in PBS at pH 7.4, whereas the neutral (protonated) **LMB** becomes relevant in the more acidic environment of cancer cells.

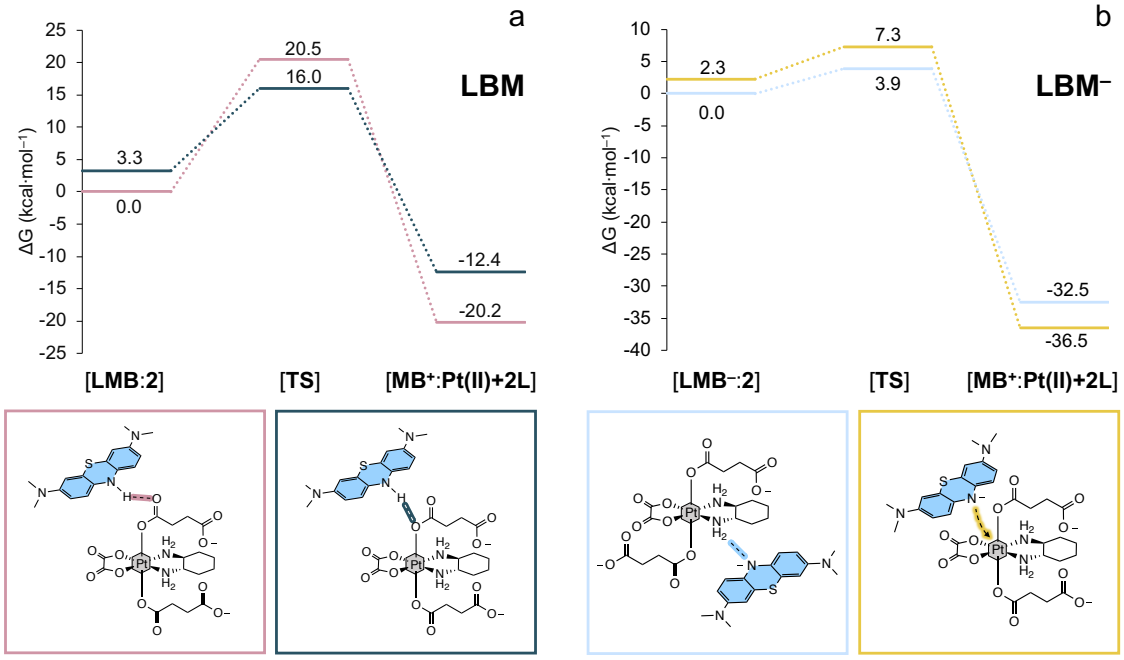

Figure 5. Free energy reaction profiles for the conversion of **2** to oxaliplatin by (a) **LMB** and (b) **LMB**$^{-}$. In the case of **LMB**, the optimized pathways involved a ligand-bridged-H transfer, mechanism, where **LMB** engages in an H-bond interaction with one succinate ligand at the carbonyl O atom or the ester O atom. For **LMB**$^{-}$, the reduction mechanisms of **2** involved an outer-sphere electron transfer and an H-bond assisted electron transfer where **LMB**$^{-}$ interacts with an amino group of the diaminocyclohexane (DACH) ligand. TS = transition state.

The reduction of **2** by **LMB** (Figure 5a) follows a ligand-bridged-H transfer mechanism as already observed for other reducing agents.[42] Two pathways were explored, each involving H-bonds between the N–H of **LMB** and either the carbonyl O or the ester O of

the Pt-coordinate succinato ligand of **2**. DFT calculations indicate that both pathways exhibit similar trends, although the one involving the formation of a bridge with the Pt-bound O atom is preferred kinetically (12.7 *vs* 20.5 kcal·mol^{-1}). The resulting product is the same for both reaction routes and is significantly stabilized compared to the initial adduct. Overall, the reduction of **2** by **LMB** is both accessible and energetically favorable.

Two free energy surfaces were also obtained for **LMB**$^{-}$ (Figure 5b). The most favorable pathway involves an H-bond assisted electron transfer where **LMB**$^{-}$ interacts with an amino group of the equatorial diaminocyclohexane (DACH) ligand. A transition state of only 3.9 kcal·mol^{-1} needs to be overcome to reach the Pt(II) product oxaliplatin. The second optimized pathway implicates an outer-sphere electron transfer with a transition state of 7.3 kcal·mol^{-1}. Both mechanisms for the two-electron reduction of **2** are highly exergonic with products thermally stabilized by over 30 kcal·mol^{-1}. These computational thermodynamic and kinetic features indicate that **LMB**$^{-}$ is an efficient Pt(IV) reducing agent.

In vitro studies

To evaluate the effectiveness of Pt prodrug activation through (photo)catalysis by **MB**$^{+}$, we initially screened the activity of all components in human cervical cancer cell lines (CaSki, SiHa, and HeLa) with integrated high-risk HPV genomes, a known risk factor for cervical cancer.[43] Pt drugs like cisplatin and carboplatin are commonly employed in clinics to treat this type of cancer, and photodynamic therapy (PDT) using various photosensitizers, including **MB**$^{+}$, is being explored as an alternative approach.[44] Previous studies by Fontana et al. demonstrated an enhanced anticancer effect with combined **MB**$^{+}$-PDT and cisplatin in these cell lines.[45] We also included the HPV-negative HaCat cell line, a model for immortalized human keratinocytes, as a non-malignant condition to broaden our understanding of the therapy's potential impact.[46] Preliminary tests (Figure S23–S26) in the dark using the whole panel of cell lines were performed to obtain the cytotoxicity profile of **MB**$^{+}$, Pt prodrugs, cisplatin and oxaliplatin at different concentrations and incubation times. Then, we selected HaCat and Caski cell lines for subsequent experiments aimed at determining the optimal light-irradiation protocol (Figure S27). None of the Pt prodrugs exhibited cytotoxicity even at the highest concentration of 100 µM across all cell lines, as observed with the reference drug oxaliplatin. In contrast, cisplatin exhibited IC_{50} values spanning from 28 to 78 µM, while the photosensitizer **MB**$^{+}$ ranged from 5 to 18 µM, aligning with findings in the existing literature.[47] Based on the results obtained, we implemented the following conditions for the administration of the compounds and photoirradiation: 100 µM **1** or **2** and 4 µM **MB**$^{+}$, 3 h of preincubation before light irradiation (followed by a thorough washing of any residual administered compounds), a light dose of 46.8 J·cm^{-2}, and 24 h of recovery before measuring cell viability. All individual components, cisplatin and oxaliplatin were also included in the tests at identical concentrations as controls.

In this setting, Pt(IV/II) derivatives and **MB**$^{+}$ did not significantly affect the viability of HaCat and CaSki cells in the absence of light (Figure 6). Cisplatin led to only a slight reduction in viability. As expected, photoirradiated **MB**$^{+}$ exhibited a PDT effect, leading to cell death, particularly noticeable in CaSki cells. This heightened effect on malignant cells was previously documented by dos Santos et al. and attributed to the distinct sub-cellular localization of **MB**$^{+}$ in cancer versus healthy cells.[48] In contrast, red light did not augment the cytotoxicity of the Pt(IV/II) compounds. A reduction in cell viability in HaCaT cells was observed when **MB**$^{+}$ was added to the Pt complexes, due to the PDT action of the catalyst alone. A distinct scenario unfolded upon combining compounds

1 and **2** with the **MB**$^+$ catalyst in CaSki cells (Figure 6). For compound **1**, statistically significant reductions in viability were observed both in the dark and upon light irradiation when compared to **MB**$^+$ alone (***P < 0.0004; one-way ANOVA followed by Bonferroni's post-test), approximately 10% and 49% respectively. These changes align with the activation of the prodrug by **MB**$^+$ inside the cell and the subsequent generation of cisplatin. When paired with the catalyst, **2** did not exhibit a comparable effect in the absence of light. However, upon light irradiation, there was a 50% decrease in cell viability with respect to **MB**$^+$ alone. As illustrated in Figure 2, compound **1** exhibits greater susceptibility to catalytic activation by **MB**$^+$ in the presence of bioreductants, particularly NADH. This discrepancy could account for the contrasting behavior observed in CaSki cells in the absence of light.

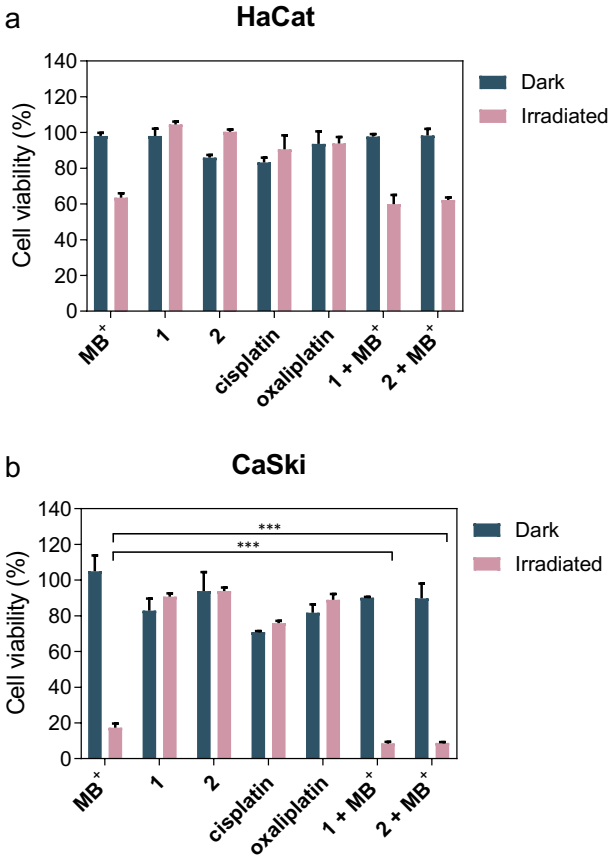

Figure 6. Cell viability in HaCat and CaSki cells treated with **1** and **2** (100 μM), either individually or combined with **MB**$^+$ (4 μM), under red light irradiation or in darkness. Cisplatin and oxaliplatin (100 μM) were tested under the same conditions as controls. In the photoirradiation experiments, cells were initially incubated with the tested compounds for 3 hours, followed by thorough washing with PBS and replacement of the culture medium prior to light exposure (λ_{exc} = 630 nm, 46.8 J·cm^{-2}). Cell viability was determined by the MTT assay at 24 h post-light treatment. Data are expressed as means ± SEM of three independent experiments (***P < 0.0004; one-way ANOVA followed by Bonferroni's post-test).

Conclusions

Pt drugs play a crucial role in cancer treatment within clinical settings. **MB**$^+$, likewise, demonstrates significant potential in chemotherapy and photochemotherapy, as evidenced by ongoing trials employing this phenothiazine derivative as an active component. Recent findings suggest that combining **MB**$^+$ as a photosensitizer with Pt

drugs such as cisplatin in integrated PDT and chemotherapy regimens can result in favorable treatment outcomes.[45]

Although the reduction in cell viability observed in our experiments is slight, this contribution underscores that the (photo)catalytic activation of Pt(IV) prodrugs by **MB**$^{+}$ may augment anticancer activity against tumoral cells, likely leveraging the synergy between the dye's PDT effect and the in-cell generation of Pt(II) drugs. The utilization of red-light excitation sources presents clinical advantages over our prior outcomes with flavin catalysts. Overall, this catalysis-based approach shows potential in mitigating the adverse side effects of Pt drugs and possibly improving the treatment effectiveness of photochemotherapy, particularly in scenarios of hypoxic conditions often found in various tumors or induced by PDT protocols.[49]
Compelling evidence suggests that Pt anticancer agents (along with other metallodrugs)[50–53] and PDT approaches[54,55] stimulate immunogenic cell death (ICD) and the release of damage-associated molecular patterns (DAMPs). We aim to explore these aspects in future research to assess whether the catalytic strategy proposed in this study could enhance the response of the immune system to cancer.

Supporting Information

Details of materials and methods, instruments, synthesis of complexes, catalysis experiments and controls, absorption spectroscopy measurements, computational modeling, and in vitro studies.

Acknowledgments

Funding for this research was received from the Spanish State Research Agency (MCIN/AEI/10.13039/501100011033, grants PID2022-139267OB-I00, FJC2021-047527-I and PID2020-114347RB-C32 to L.S., A.C.C., and V.M.M., respectively), the Basque Government (Eusko Jaurlaritza Grant PIBA_2021_1_0034 and IT1639-22, to L.S. and V.M.M.), the University of the Basque Country (EHU-G23/03), the University of Turin (RILO 2022 and RILO 2023, V.D.O and M.D.A.; Grant for Internationalization – GFI 2022, V.D.O.), the University of Calabria, the Italian Ministry of Education and Research (PRIN Project 2022S3AZCC, V.D.O.), the European Union with the MUR PNRR Extended Partnership initiative on Emerging Infectious Diseases (Project No. PE00000007, INF-ACT, M.D.A.). DIPC received support from the “Severo Ochoa” Programme for Centres of Excellence in R&D (MINECO, Grants CEX2018-000867-S). S.S. and E.S. thank the financial support from ICSC – Centro Nazionale di Ricerca in High Performance Computing, Big Data and Quantum Computing, funded by European Union – NextGenerationEU – PNRR, Missione 4 Componente 2 Investimento 1.4. We thank Dr. José Ignacio Miranda (SGIKER, UPV/EHU) for his technical support with ^{195}Pt NMR experiments.

References

(1) Destito, P.; Vidal, C.; López, F.; Mascareñas, J. L. Transition Metal-Promoted Reactions in Aqueous Media and Biological Settings. *Chem. - A Eur. J.* **2021**, *27* (15), 4789–4816. https://doi.org/10.1002/chem.202003927.

(2) Ngo, A. H.; Bose, S.; Do, L. H. Intracellular Chemistry: Integrating Molecular Inorganic Catalysts with Living Systems. *Chem. – A Eur. J.* **2018**, *24* (42), 10584–10594. https://doi.org/10.1002/chem.201800504.

(3) Soldevila-Barreda, J. J.; Metzler-Nolte, N. Intracellular Catalysis with Selected Metal Complexes and Metallic Nanoparticles: Advances toward the Development of Catalytic Metallodrugs. *Chem. Rev.* **2019**, *119* (2), 829–869. https://doi.org/10.1021/acs.chemrev.8b00493.

(4) Soldevila-Barreda, J. J.; Sadler, P. J. Approaches to the Design of Catalytic Metallodrugs. *Curr. Opin. Chem. Biol.* **2015**, *25*, 172–183. https://doi.org/10.1016/j.cbpa.2015.01.024.

(5) Yu, Z.; Cowan, J. A. Catalytic Metallodrugs: Substrate-Selective Metal Catalysts as Therapeutics. *Chem. – A Eur. J.* **2017**, *23* (57), 14113–14127. https://doi.org/10.1002/chem.201701714.

(6) Alonso-de Castro, S.; Terenzi, A.; Gurruchaga-Pereda, J.; Salassa, L. Catalysis Concepts in Medicinal Inorganic Chemistry. *Chem. - A Eur. J.* **2019**, *25* (27), 6651–6660. https://doi.org/10.1002/chem.201806341.

(7) He, X.; Zeng, T.; Li, Z.; Wang, G.; Ma, N. Catalytic Molecular Imaging of MicroRNA in Living Cells by DNA-Programmed Nanoparticle Disassembly. *Angew. Chem. Int. Ed.* **2016**, *55* (9), 3073–3076. https://doi.org/https://doi.org/10.1002/anie.201509726.

(8) Vickerman, B. M.; Zywot, E. M.; Tarrant, T. K.; Lawrence, D. S. Taking Phototherapeutics from Concept to Clinical Launch. *Nat. Rev. Chem.* **2021**, *5* (11), 816–834. https://doi.org/10.1038/s41570-021-00326-w.

(9) Joyner, J. C.; Hocharoen, L.; Cowan, J. A. Targeted Catalytic Inactivation of Angiotensin Converting Enzyme by Lisinopril-Coupled Transition-Metal Chelates. *J. Am. Chem. Soc.* **2012**, *134* (7), 3396–3410. https://doi.org/10.1021/ja208791f.

(10) Jin, Y.; Cowan, J. A. Cellular Activity of Rev Response Element RNA Targeting Metallopeptides. *J. Biol. Inorg. Chem.* **2007**, *12* (5), 637–644. https://doi.org/10.1007/s00775-007-0221-2.

(11) Alcalde-Ordóñez, A.; Barreiro-Piñeiro, N.; McGorman, B.; Gómez-González, J.; Bouzada, D.; Rivadulla, F.; Vázquez, M. E.; Kellett, A.; Martínez-Costas, J.; López, M. V. A Copper(Ii) Peptide Helicate Selectively Cleaves DNA Replication Foci in Mammalian Cells. *Chem. Sci.* **2023**, *14* (48), 14082–14091. https://doi.org/10.1039/D3SC03303A.

(12) Coverdale, J. P. C. C.; Romero-Canelón, I.; Sanchez-Cano, C.; Clarkson, G. J.; Habtemariam, A.; Wills, M.; Sadler, P. J. Asymmetric Transfer Hydrogenation by Synthetic Catalysts in Cancer Cells. *Nat. Chem.* **2018**, *10* (3), 347–354. https://doi.org/10.1038/nchem.2918.

(13) Soldevila-Barreda, J. J.; Romero-Canelón, I.; Habtemariam, A.; Sadler, P. J. Transfer Hydrogenation Catalysis in Cells as a New Approach to Anticancer Drug Design. *Nat. Commun.* **2015**, *6*, 6582. https://doi.org/10.1038/ncomms7582.

(14) Dougan, S. J.; Habtemariam, A.; McHale, S. E.; Parsons, S.; Sadler, P. J. Catalytic Organometallic Anticancer Complexes. *Proc. Natl. Acad. Sci.* **2008**, *105* (33), 11628–

11633. https://doi.org/10.1073/pnas.0800076105.

(15) Alonso-de Castro, S.; Ruggiero, E.; Ruiz-de-Angulo, A.; Rezabal, E.; Mareque-Rivas, J. C.; Lopez, X.; López-Gallego, F.; Salassa, L. Riboflavin as a Bioorthogonal Photocatalyst for the Activation of a Pt^{IV} Prodrug. *Chem. Sci.* **2017**, *8* (6), 4619–4625. https://doi.org/10.1039/C7SC01109A.

(16) Alonso-de Castro, S.; Cortajarena, A. L.; López-Gallego, F.; Salassa, L. Bioorthogonal Catalytic Activation of Platinum and Ruthenium Anticancer Complexes by FAD and Flavoproteins. *Angew. Chem. Int. Ed.* **2018**, *57* (12), 3143–3147. https://doi.org/10.1002/anie.201800288.

(17) Gurruchaga-Pereda, J.; Martínez-Martínez, V.; Formoso, E.; Azpitarte, O.; Rezabal, E.; Lopez, X.; Cortajarena, A. L.; Salassa, L. Enhancing the Photocatalytic Conversion of Pt(IV) Substrates by Flavoprotein Engineering. *J. Phys. Chem. Lett.* **2021**, *12* (19), 4504–4508. https://doi.org/10.1021/acs.jpclett.1c00802.

(18) Mazzei, L. F.; Gurruchaga-Pereda, J.; Martínez, Á.; Martínez, J. C.; Salassa, L.; Cortajarena, A. L. Engineered Flavoproteins as Bioorthogonal Photo-Triggers for the Activation of Metal-Based Anticancer Prodrugs. *Chem. Commun.* **2023**, *59* (32), 4754–4757. https://doi.org/10.1039/d2cc06363h.

(19) Velasco-Lozano, S.; Castro, S. A. De; Sanchez-Cano, C.; Benítez-Mateos, A. I.; López-Gallego, F.; Salassa, L. Metal Substrate Catalysis in the Confined Space for Platinum Drug Delivery. *Chem. Sci.* **2022**, *13* (1), 59–67. https://doi.org/10.1039/d1sc05151b.

(20) Gurruchaga-Pereda, J.; Martínez-Martínez, V.; Rezabal, E.; Lopez, X.; Garino, C.; Mancin, F.; Cortajarena, A. L.; Salassa, L. Flavin Bioorthogonal Photocatalysis Toward Platinum Substrates. *ACS Catal.* **2020**, *10* (1), 187–196. https://doi.org/10.1021/acscatal.9b02863.

(21) López-Gallego, F.; Salassa, L. Catalysis toward Metal-Based Substrates: A New Prospect for Inorganic Chemistry. *Chem Catal.* **2023**, *3* (2), 100459. https://doi.org/https://doi.org/10.1016/j.checat.2022.10.035.

(22) Haouzi, P.; Gueguinou, M.; Sonobe, T.; Judenherc-Haouzi, A.; Tubbs, N.; Trebak, M.; Cheung, J.; Bouillaud, F. Revisiting the Physiological Effects of Methylene Blue as a Treatment of Cyanide Intoxication. *Clin. Toxicol.* **2018**, *56* (9), 828–840. https://doi.org/10.1080/15563650.2018.1429615.

(23) Boltes Cecatto, R.; Siqueira de Magalhães, L.; Fernanda Setúbal Destro Rodrigues, M.; Pavani, C.; Lino-dos-Santos-Franco, A.; Teixeira Gomes, M.; Fátima Teixeira Silva, D. Methylene Blue Mediated Antimicrobial Photodynamic Therapy in Clinical Human Studies: The State of the Art. *Photodiagnosis Photodyn. Ther.* **2020**, *31*, 101828. https://doi.org/10.1016/j.pdpdt.2020.101828.

(24) Oz, M.; Lorke, D. E.; Petroianu, G. A. Methylene Blue and Alzheimer's Disease. *Biochem. Pharmacol.* **2009**, *78* (8), 927–932. https://doi.org/10.1016/j.bcp.2009.04.034.

(25) Iolascon, A.; Bianchi, P.; Andolfo, I.; Russo, R.; Barcellini, W.; Fermo, E.; Toldi, G.; Ghirardello, S.; Rees, D.; Van Wijk, R.; et al. Recommendations for Diagnosis and Treatment of Methemoglobinemia. *Am. J. Hematol.* **2021**, *96* (12), 1666–1678. https://doi.org/10.1002/ajh.26340.

(26) Tummers, Q. R. J. G.; Verbeek, F. P. R.; Schaafsma, B. E.; Boonstra, M. C.; Van Der Vorst, J. R.; Liefers, G. J.; Van De Velde, C. J. H.; Frangioni, J. V.; Vahrmeijer, A. L. Real-Time Intraoperative Detection of Breast Cancer Using near-Infrared Fluorescence Imaging and Methylene Blue. *Eur. J. Surg. Oncol.* **2014**, *40* (7), 850–858. https://doi.org/10.1016/j.ejso.2014.02.225.

(27) Tardivo, J. P.; Del Giglio, A.; De Oliveira, C. S.; Gabrielli, D. S.; Junqueira, H. C.; Tada, D. B.; Severino, D.; De Fátima Turchiello, R.; Baptista, M. S. Methylene Blue in Photodynamic Therapy: From Basic Mechanisms to Clinical Applications. *Photodiagnosis Photodyn. Ther.* **2005**, *2* (3), 175–191. https://doi.org/10.1016/S1572-1000(05)00097-9.

(28) https://clinicaltrials.gov/search?term=Methylene Blue&cond=Cancer.

(29) Sánchez-Camacho, J.; Infante-Tadeo, S.; Carrasco, A. C.; Scoditti, S.; Martínez, Á.; Barroso-Bujans, F.; Sicilia, E.; Pizarro, A. M.; Salassa, L. Flavin-Conjugated Pt(IV) Anticancer Agents. *Inorg. Chem.* **2023**, *62* (14), 5644–5651. https://doi.org/10.1021/acs.inorgchem.3c00193.

(30) Kelner, M. J.; Alexander, N. M. Methylene Blue Directly Oxidizes Glutathione without the Intermediate Formation of Hydrogen Peroxide. *J. Biol. Chem.* **1985**, *260* (28), 15168–15171. https://doi.org/10.1016/S0021-9258(18)95717-0.

(31) Alonso-de Castro, S.; Terenzi, A.; Hager, S.; Englinger, B.; Faraone, A.; Martínez, J. C.; Galanski, M.; Keppler, B. K.; Berger, W.; Salassa, L. Biological Activity of PtIV Prodrugs Triggered by Riboflavin-Mediated Bioorthogonal Photocatalysis. *Sci. Rep.* **2018**, *8* (1), 17198. https://doi.org/10.1038/s41598-018-35655-2.

(32) Infante, I.; Azpiroz, J. M.; Blanco, N. G.; Ruggiero, E.; Ugalde, J. M.; Mareque-Rivas, J. C.; Salassa, L. Quantum Dot Photoactivation of Pt(IV) Anticancer Agents: Evidence of an Electron Transfer Mechanism Driven by Electronic Coupling. *J. Phys. Chem. C* **2014**, *118* (16), 8712–8721. https://doi.org/10.1021/jp501447q.

(33) Anderson, L.; Wittkopp, S. M.; Painter, C. J.; Liegel, J. J.; Schreiner, R.; Bell, J. A.; Shakhashiri, B. Z. What Is Happening When the Blue Bottle Bleaches: An Investigation of the Methylene Blue-Catalyzed Air Oxidation of Glucose. *J. Chem. Educ.* **2012**, *89* (11), 1425–1431. https://doi.org/10.1021/ed200511d.

(34) Dean, J. C.; Oblinsky, D. G.; Rafiq, S.; Scholes, G. D. Methylene Blue Exciton States Steer Nonradiative Relaxation: Ultrafast Spectroscopy of Methylene Blue Dimer. *J. Phys. Chem. B* **2016**, *120* (3), 440–454. https://doi.org/10.1021/acs.jpcb.5b11847.

(35) Chen, J.; Cesario, T. C.; Rentzepis, P. M. Time Resolved Spectroscopic Studies of Methylene Blue and Phenothiazine Derivatives Used for Bacteria Inactivation. *Chem. Phys. Lett.* **2010**, *498* (1–3), 81–85. https://doi.org/10.1016/j.cplett.2010.08.042.

(36) Alarcón, E.; Edwards, A. M.; Aspee, A.; Moran, F. E.; Borsarelli, C. D.; Lissi, E. A.; Gonzalez-Nilo, D.; Poblete, H.; Scaiano, J. C. Photophysics and Photochemistry of Dyes Bound to Human Serum Albumin Are Determined by the Dye Localization. *Photochem. Photobiol. Sci.* **2010**, *9* (1), 93–102. https://doi.org/10.1039/b9pp00091g.

(37) Haynes, R. K.; Chan, W. C.; Wong, H. N.; Li, K. Y.; Wu, W. K.; Fan, K. M.; Sung, H. H. Y.; Williams, I. D.; Prosperi, D.; Melato, S.; et al. Facile Oxidation of Leucomethylene Blue and Dihydroflavins by Artemisinins: Relationship with Flavoenzyme Function and Antimalarial Mechanism of Action. *ChemMedChem* **2010**, *5* (8), 1282–1299. https://doi.org/10.1002/cmdc.201000225.

(38) Hirakawa, K.; Mori, M. Phenothiazine Dyes Induce NADH Photooxidation through Electron Transfer: Kinetics and the Effect of Copper Ions. *ACS Omega* **2021**, *6* (12), 8630–8636. https://doi.org/10.1021/acsomega.1c00484.

(39) Scoditti, S.; Dabbish, E.; Pieslinger, G. E.; Rezabal, E.; Lopez, X.; Sicilia, E.; Salassa, L. Flavin-Mediated Photoactivation of Pt(IV) Anticancer Complexes: Computational Insights

on the Catalytic Mechanism. *Phys. Chem. Chem. Phys.* **2022**, *24* (9), 5323–5329. https://doi.org/10.1039/D1CP05507K.

(40) Impert, O.; Katafias, A.; Kita, P.; Mills, A.; Pietkiewicz-Graczyk, A.; Wrzeszcz, G. Kinetics and Mechanism of a Fast Leuco-Methylene Blue Oxidation by Copper(Ii)–Halide Species in Acidic Aqueous Media. *J. Chem. Soc. Dalton Trans.* **2003**, *3* (3), 348–353. https://doi.org/10.1039/b205786g.

(41) Aguirre-Soto, A.; Lim, C. H.; Hwang, A. T.; Musgrave, C. B.; Stansbury, J. W. Visible-Light Organic Photocatalysis for Latent Radical-Initiated Polymerization via $2e^-/1H^+$ Transfers: Initiation with Parallels to Photosynthesis. *J. Am. Chem. Soc.* **2014**, *136* (20), 7418–7427. https://doi.org/10.1021/ja502441d.

(42) Ponte, F.; Scoditti, S.; Mazzone, G.; Sicilia, E. The Current Status in Computational Exploration of Pt(IV) Prodrug Activation by Reduction. *Phys. Chem. Chem. Phys.* **2023**, *25* (23), 15586–15599. https://doi.org/10.1039/D3CP01150J.

(43) Okunade, K. S. Human Papillomavirus and Cervical Cancer. *J. Obstet. Gynaecol. (Lahore).* **2020**, *40* (5), 602–608. https://doi.org/10.1080/01443615.2019.1634030.

(44) López-Cárdenas, M. T.; Jiménez, A.; Espinosa-Montesinos, A.; Maldonado-Alvarado, E.; Osorio-Peralta, M. O.; Martinez-Escobar, A.; Moreno-Vázquez, A.; Aguilera-Arreola, M. G.; Ramón-Gallegos, E. Elimination of Human Papillomavirus and Cervical Pathological Microbiota with Photodynamic Therapy in Women from Mexico City with Cervical Intraepithelial Neoplasia I. *Photochem. Photobiol.* **2023**, *99* (6), 1468–1475. https://doi.org/https://doi.org/10.1111/php.13791.

(45) De Freitas, L. M.; Soares, C. P.; Fontana, C. R. Synergistic Effect of Photodynamic Therapy and Cisplatin: A Novel Approach for Cervical Cancer. *J. Photochem. Photobiol. B Biol.* **2014**, *140*, 365–373. https://doi.org/10.1016/j.jphotobiol.2014.08.021.

(46) Boukamp, P.; Petrussevska, R. T.; Breitkreutz, D.; Hornung, J.; Markham, A.; Fusenig, N. E. Normal Keratinization in a Spontaneously Immortalized Aneuploid Human Keratinocyte Cell Line. *J. Cell Biol.* **1988**, *106* (3), 761–771. https://doi.org/10.1083/jcb.106.3.761.

(47) Wainwright, M.; Phoenix, D. A.; Rice, L.; Burrow, S. M.; Waring, J. Increased Cytotoxicity and Phototoxicity in the Methylene Blue Series via Chromophore Methylation. *J. Photochem. Photobiol. B Biol.* **1997**, *40* (3), 233–239. https://doi.org/10.1016/S1011-1344(97)00061-4.

(48) dos Santos, A. F.; Terra, L. F.; Wailemann, R. A. M.; Oliveira, T. C.; de Morais Gomes, V.; Mineiro, M. F.; Meotti, F. C.; Bruni-Cardoso, A.; Baptista, M. S.; Labriola, L. Methylene Blue Photodynamic Therapy Induces Selective and Massive Cell Death in Human Breast Cancer Cells. *BMC Cancer* **2017**, *17* (1), 1–15. https://doi.org/10.1186/s12885-017-3179-7.

(49) Zhang, C.; Hu, X.; Jin, L.; Lin, L.; Lin, H.; Yang, Z.; Huang, W. Strategic Design of Conquering Hypoxia in Tumor for Advanced Photodynamic Therapy. *Adv. Healthc. Mater.* **2023**, *12*, e2300530. https://doi.org/10.1002/adhm.202300530.

(50) Englinger, B.; Pirker, C.; Heffeter, P.; Terenzi, A.; Kowol, C. R.; Keppler, B. K.; Berger, W. Metal Drugs and the Anticancer Immune Response. *Chem. Rev.* **2019**, *119* (2), 1519–1624. https://doi.org/10.1021/acs.chemrev.8b00396.

(51) Terenzi, A.; Pirker, C.; Keppler, B. K.; Berger, W. Anticancer Metal Drugs and Immunogenic Cell Death. *J. Inorg. Biochem.* **2016**, *165*, 71–79. https://doi.org/https://doi.org/10.1016/j.jinorgbio.2016.06.021.

(52) Sen, S.; Won, M.; Levine, M. S.; Noh, Y.; Sedgwick, A. C.; Kim, J. S.; Sessler, J. L.; Arambula, J. F. Metal-Based Anticancer Agents as Immunogenic Cell Death Inducers: The Past, Present, and Future. *Chem. Soc. Rev.* **2022**, *51* (4), 1212–1233. https://doi.org/10.1039/d1cs00417d.

(53) Zhang, L.; Montesdeoca, N.; Karges, J.; Xiao, H. Immunogenic Cell Death Inducing Metal Complexes for Cancer Therapy. *Angew. Chem. Int. Ed.* **2023**, *62*, e202300662. https://doi.org/10.1002/anie.202300662.

(54) Falk-Mahapatra, R.; Gollnick, S. O. Photodynamic Therapy and Immunity: An Update. *Photochem. Photobiol.* **2020**, *96* (3), 550–559. https://doi.org/10.1111/php.13253.

(55) Konda, P.; Lifshits, L. M.; Roque, J. A.; Cole, H. D.; Cameron, C. G.; McFarland, S. A.; Gujar, S. Discovery of Immunogenic Cell Death-Inducing Ruthenium-Based Photosensitizers for Anticancer Photodynamic Therapy. *Oncoimmunology* **2021**, *10* (1), 2–5. https://doi.org/10.1080/2162402X.2020.1863626.